

RESEARCH ARTICLE | NOVEMBER 19 2024

## Fundamental optical transitions in hexagonal boron nitride epilayers

J. Li ; J. Y. Lin ; H. X. Jiang  



*APL Mater.* 12, 111115 (2024)

<https://doi.org/10.1063/5.0234673>



### Articles You May Be Interested In

Layer number dependent optical properties of multilayer hexagonal BN epilayers

*Appl. Phys. Lett.* (February 2017)

Carbon-related donor–acceptor pair transition in the infrared in h-BN

*Appl. Phys. Lett.* (March 2024)

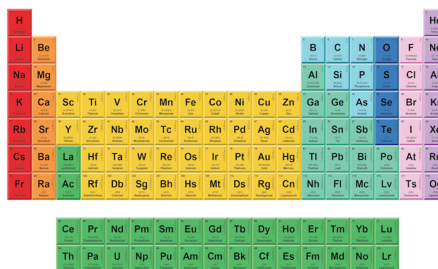
Chemical vapor deposition of  $sp^2$ -boron nitride on Si(111) substrates from triethylboron and ammonia: Effect of surface treatments

*J. Vac. Sci. Technol. A* (May 2020)



THE MATERIALS SCIENCE MANUFACTURER®

**Now Invent.™**



American Elements  
Opens a World of Possibilities

...Now Invent!

[www.americanelements.com](http://www.americanelements.com)

© 2021-2024 American Elements & U.S. Registered Trademark

# Fundamental optical transitions in hexagonal boron nitride epilayers

Cite as: APL Mater. 12, 111115 (2024); doi: 10.1063/5.0234673  
Submitted: 22 August 2024 • Accepted: 5 November 2024 •  
Published Online: 19 November 2024



View Online



Export Citation



CrossMark

J. Li,  J. Y. Lin,  and H. X. Jiang<sup>a)</sup> 

## AFFILIATIONS

Department of Electrical and Computer Engineering, Texas Tech University, Lubbock, Texas 79409, USA

<sup>a)</sup> Author to whom correspondence should be addressed: [hx.jiang@ttu.edu](mailto:hx.jiang@ttu.edu)

## ABSTRACT

Fundamental optical transitions in hexagonal boron nitride (h-BN) epilayers grown on sapphire by metal–organic chemical vapor deposition (MOCVD) using triethylboron as the boron precursor have been probed by photoluminescence (PL) emission spectroscopy. The low temperature (10 K) PL spectrum exhibits two groups of emission lines. The first group includes the direct observation of the free exciton and impurity bound exciton (BX) transitions and phonon replicas of the BX transition, whereas the second group is attributed to the direct observation of the band-to-band transition and its associated phonon replicas. The observations of zero-phonon lines of the band-to-band and exciton transitions, which are supposedly forbidden or “dark” in perfect h-BN crystals, result from a relaxed requirement of momentum conservation due to symmetry-breaking in the presence of high concentrations of impurities/defects and strain, which in turn provided more deterministic values of the energy bandgap ( $E_g$ ), exciton binding energy ( $E_x$ ), and binding energy of impurity bound excitons ( $E_{BX}$ ) in h-BN epilayers. Excitonic parameters of h-BN epilayers grown by MOCVD, carbon-free chemical vapor deposition, and high purity h-BN bulk materials are compared and discussed. The present results, together with available information in the literature, represent a significant improvement in the understanding of the fundamental optical properties and excitonic parameters of h-BN ultrawide bandgap semiconductors.

© 2024 Author(s). All article content, except where otherwise noted, is licensed under a Creative Commons Attribution (CC BY) license (<https://creativecommons.org/licenses/by/4.0/>). <https://doi.org/10.1063/5.0234673>

Hexagonal boron nitride (h-BN) has attracted much interest recently, largely because of its potential applications in 2D structures serving as a substrate and dielectric/gate layer,<sup>1–3</sup> single photon emitters and quantum qubits,<sup>4–6</sup> deep-ultraviolet (DUV) photonics,<sup>7–10</sup> and neutron detectors.<sup>11–14</sup> It is well established that all figures of merit (or the overall performance) of semiconductor electronic devices scale with the material’s energy bandgap,  $E_g$ , in a highly non-linear manner.<sup>15</sup> As such, h-BN is also expected to expand its capabilities into the area of power electronics due to its ultrawide bandgap (UWBG) of about 6.1 eV. With a worldwide effort taking place during the last decade, tremendous progress has been made in advancing h-BN materials growth, basic property understanding, and device applications.

The band-edge photoluminescence (PL) emission properties of h-BN have been investigated for h-BN bulk materials synthesized by high pressure and high temperature (HPHT) and metal flux solution methods,<sup>16–22</sup> as well as for epilayers grown by different epitaxial growth methods.<sup>23,24</sup> It is now established that h-BN is an UWBG

semiconductor with an indirect energy gap of around 6.1 eV at 10 K with the conduction band minimum (CBM) at M-point and valence band maximum (VBM) at K-point in the first Brillouin zone (BZ).<sup>20,25–27</sup> As such, direct band-to-band and excitonic transitions in h-BN are expected to be invisible or “dark.” Due to its unique crystalline and electronic structures, the material system is known to exhibit an unusually strong phonon and charge carrier interaction, leading to very efficient optical transitions near the band-edge, assisted by phonons to satisfy the conservation of momentum.<sup>20</sup> However, many optical properties and fundamental parameters are still unknown. For example, the reported excitonic parameters, such as free and impurity bound exciton binding energies, have large variations. These parameters were often deduced indirectly from different types of materials and different measurement techniques, which unavoidably resulted in large uncertainties. As with other semiconductor materials in their early development stages, understanding the fundamental optical transitions and excitonic parameters is critical for further advancing h-BN semiconductor material and device technologies.

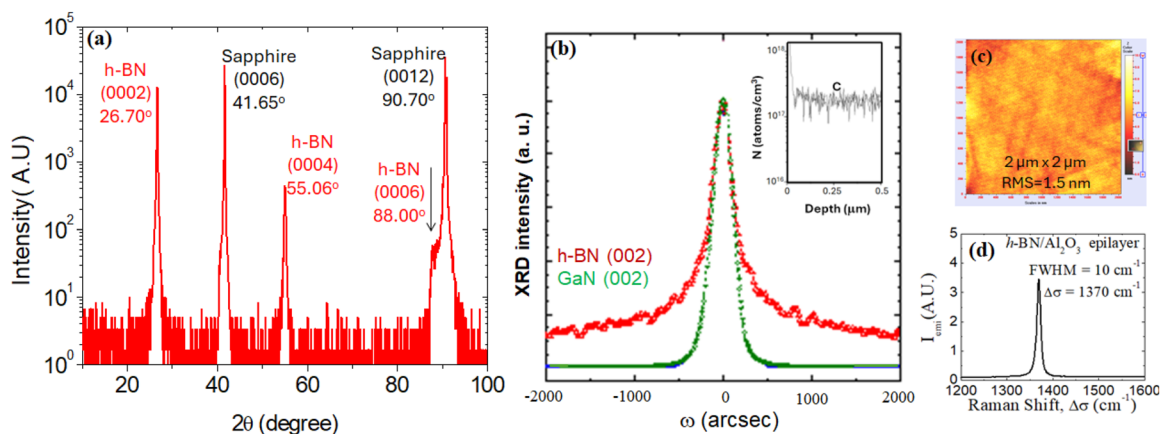
We present here the results of a detailed study of fundamental optical transitions in h-BN epilayers probed by low temperature PL emission spectroscopy. Epitaxial layers of h-BN of 1  $\mu\text{m}$  in thickness were grown by MOCVD on c-plane sapphire using triethylboron (TEB) and ammonia ( $\text{NH}_3$ ) as precursors for B and N, respectively, and hydrogen as a carrier gas. The epilayers were grown at 1350  $^\circ\text{C}$  using an optimized pulsed precursor flow epitaxy technique we developed previously to minimize the parasitic reaction between TEB and  $\text{NH}_3$  at a growth rate of 0.5  $\mu\text{m}/\text{h}$ .<sup>24</sup> The growth rate was observed to be proportional to the TEB flow rate. Structural properties were characterized by x-ray diffraction (XRD) and Raman measurements. The photoluminescence (PL) spectroscopy system employed in this study consists of a frequency quadrupled Ti: sapphire laser with an excitation wavelength set at 197 nm and a monochromator (1.3 m). A single photon counting detection system together with a micro-channel-plate photo-multiplier tube (PMT) was used to record the PL spectra.<sup>18,19</sup>

The x-ray diffraction (XRD) pattern (in XRD  $2\theta$ - $\omega$  scans) measured in a large angle range is plotted in Fig. 1(a), clearly revealing diffraction peaks resulting from h-BN (0002), (0004), and (0006) stacked planes in the c-direction. The measured h-BN (0002) peak is centered at  $2\theta = 26.70^\circ$ , corresponding to a c-lattice constant of 6.68 ( $\text{\AA}$ ).<sup>28</sup> Figure 1(b) compares the XRD measurement results in  $\omega$ -scans (rocking curves) of the (0002) diffraction peaks among GaN and h-BN epilayers produced by MOCVD. The results revealed that the h-BN epilayers employed in this work have an XRD rocking curve of full width at half maximum (FWHM) of  $\sim 375$  arcsec, which is comparable to the FWHM of about 290 arcsec for GaN epilayers. XRD results thus indicate that h-BN epilayers studied here possess an excellent long-range order along the c-axis but contain a comparable density of defects (or stacking faults in the case of h-BN with a layered crystalline structure) as that in GaN epilayers deposited on sapphire (typically  $> 10^{10} \text{ cm}^{-2}$ ).<sup>29</sup> As shown in Fig. 1(c), the surface morphology of the as-grown h-BN epilayer is acceptable by exhibiting an RMS roughness of  $\sim 1.5$  nm in an

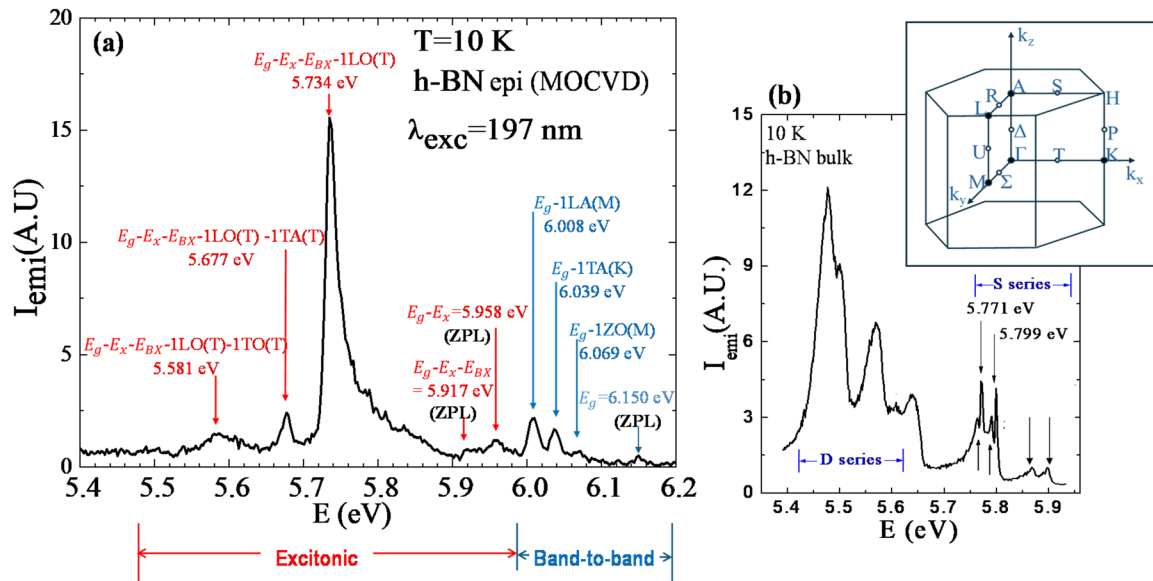
atomic force microscopy (AFM) image scanned over a  $2 \times 2 \mu\text{m}^2$  area.

Figure 1(d) shows the room temperature Raman spectrum of a representative h-BN epilayer. It is worth noting that the observed Raman peak in this epilayer is shifted to a higher phonon frequency of  $\Delta\sigma = 1370 \text{ cm}^{-1}$  with respect to  $\Delta\sigma = 1366 \text{ cm}^{-1}$  expected for the  $E_{2g}$  in-plane shear mode in bulk h-BN.<sup>30</sup> It is well documented that strain induced by the substrate can cause a shift in the Raman spectral peak.<sup>31</sup> The Raman spectrum, therefore, indicates that thin epitaxial layers deposited on sapphire are under strain. The observed spectral linewidth of  $10 \text{ cm}^{-1}$  is slightly larger than a typical value observed in HPHT grown small bulk crystals of  $8 \text{ cm}^{-1}$ .<sup>30</sup>

The band-edge PL emission properties of h-BN have been studied for quite some time for bulk crystals synthesized by HPHT as well as by metal flux solution methods<sup>16–22</sup> and more recently for h-BN epilayers synthesized by chemical vapor deposition (CVD) using carbon free precursors.<sup>23</sup> It has been universally observed that the low temperature band-edge PL spectrum of high-purity h-BN bulk materials consists of two groups of optical transitions: multiple sharp peaks designated as the S (sharp) lines in the spectral range of 5.75–5.95 eV and more diffused bands labeled as D lines in the spectral range of 5.4–5.7 eV.<sup>16–22</sup> The transition mechanisms of these optical transitions have been investigated and thoroughly understood.<sup>20–23</sup> Because h-BN has an indirect energy bandgap, it is well established now that the observed S- and D-lines in h-BN bulk crystals involve free exciton transitions assisted by longitudinal optical/transverse optical (LO/TO) as well as by other phonons at T-point in the first BZ to satisfy the requirement of momentum conservation.<sup>20–23</sup> Moreover, the exciton related transition lines assisted by LO/TO phonons tend to exhibit the highest emission intensities because the exciton-LO/TO phonon interaction is the strongest.<sup>20–23</sup> This hallmark feature can be utilized to identify the nature of near band-edge optical transitions in h-BN epilayers studied here.



**FIG. 1.** (a) XRD spectra in  $2\theta$ - $\omega$  scan. (b) Comparison of XRD rocking curves of (0002) diffraction peaks among GaN and h-BN epilayers deposited on sapphire by MOCVD. The inset plots the carbon concentration as a function of the h-BN epilayer depth probed by SIMS. (c) AFM image of a h-BN epilayer deposited on sapphire. (d) Raman spectrum of a h-BN epilayer deposited on sapphire.



**FIG. 2.** (a) Low temperature (10 K) PL spectrum of a h-BN epilayer used in this study. The observed “excitonic” group (red color) consists of FX and BX zero-phonon (ZPL) lines at  $E_g - E_x = 5.958$  eV and  $E_g - E_x - E_{BX} = 5.917$  eV, respectively, and phonon replicas of the BX transition, with the BX + 1LO(T) being the most dominant emission peak appearing at  $E_g - E_x - E_{BX} - 1LO(T) = 5.734$  eV. The observed “band-to-band” group (blue color) consists of the band-to-band ZPL at  $E_g$  and its phonon replicas. All zero-phonon lines are identified with ZPL. (b) A low temperature (10 K) photoluminescence emission spectrum of an h-BN bulk crystal including both the S-series and D-series emission lines [figure reproduced from Fig. 2(a) of Li *et al.*, “Nature of exciton transitions in hexagonal boron nitride,” *Appl. Phys. Lett.* **108**, 122101 (2016). Copyright 2016 AIP Publishing LLC.] and inset is a schematic illustration of the first BZ and several high symmetry points of the first BZ in h-BN.

Figure 2(a) shows a low temperature (10 K) PL spectrum of a h-BN epilayer used in this study, which is quite different from those of h-BN bulk materials<sup>16–22</sup> in terms of the dominant peak positions as well as the spectral line shape. For comparison, Fig. 2(b) shows a typical low temperature (10 K) PL emission spectrum of a h-BN bulk crystal sample synthesized by metal flux solution methods,<sup>19</sup> which exhibits both the well-known S-series and D-series lines. The spectrum shown in Fig. 2(a) exhibits a dominant transition at 5.734 eV. Most prominently, the sharp transition lines (or the S-bands) involving the multiple free exciton transitions assisted by phonons appearing in the spectral range of 5.75–5.95 eV observed in h-BN bulk materials are absent in h-BN epilayers studied here.

By carefully inspecting the spectrum shown in Fig. 2(a), two groups of emission lines can be identified, which are labeled with different colors. The first “excitonic” group, consisting of five emission lines marked with red, is at 5.958, 5.917, 5.734, 5.677, and 5.581 eV. Among these five emission lines, the 5.734 eV peak has the highest intensity with a line shape that differs from those of the S-lines observed in h-BN bulk materials. We believe that all these five emission lines are related to zero-phonon lines (ZPL) of the free-exciton (FX) and bound-exciton (BX) transitions and the phonon replicas of the BX transition. More specifically, we assign the two weakest emission peaks at 5.958 and 5.917 eV in the “excitonic” group to the zero-phonon lines (ZPL) of free exciton (FX) and impurity bound exciton (BX), with emission peak positions at  $E_g - E_x = 5.958$  eV and  $E_g - E_x - E_{BX} = 5.917$  eV, respectively, where  $E_x$  denotes the free exciton binding energy and  $E_{BX}$  denotes the impurity bound exciton binding energy. The second “band-to-band”

group consists of weaker emission lines at 6.150, 6.069, 6.039, and 6.008 eV marked with blue color. We believe that this group is related to the ZPL of the band-to-band transition with emission peak position marked as  $E_g$  as well as its phonon replicas. We discuss a few important features revealed in Fig. 2(a) below based on which the physical origins of the observed emission lines can be fully understood.

First, the h-BN epilayers studied here are expected to contain carbon impurities, which were unavoidably incorporated from the TEB precursor during growth. Indeed, the concentration of residual carbon revealed by secondary ion mass spectrometry (SIMS) measurement shown in the inset of Fig. 1(b) is about  $2 \times 10^{17} \text{ cm}^{-3}$ . Based on the spectral peak positions and line shape, the strongest emission peak can be decisively assigned to the impurity bound exciton (BX) transition assisted by LO phonons because the exciton-LO/TO phonon interaction is the strongest in h-BN, analogous to the case in h-BN bulk materials<sup>20–22</sup> and epilayers produced by carbon-free CVD,<sup>23</sup> in which the free exciton transitions assisted by LO/TO phonons are dominant. The inset of Fig. 2(b) shows a schematic illustration of the first BZ and several high symmetry points in the BZ in h-BN. Table I lists phonon energies (in units of meV) of different modes at various high symmetry points in the first BZ.<sup>32</sup> In correspondence with the phonons involved in the free exciton transitions observed in high purity h-BN bulk materials<sup>20–22</sup> and epilayers produced by carbon-free CVD<sup>23</sup> as well as phonon energies listed in Table I, the physical origins for each transition line in the “excitonic” group in Fig. 2(a) can be identified, whereby every phonon participating in the “excitonic” group

**TABLE I.** List of energies (in meV) of phonons at various high symmetry points in the first BZ in h-BN.<sup>32</sup>

	$\Gamma$	M	K	T
LO	200	163	160	180–185
TO	170	158	165	155–162
ZO	92–99	81	71	83–90
LA	7	142	135	85–92
TA	0	68	110	66
ZA	0–15	39	40	23

involves a T-point in the first BZ. These include the BX transition assisted by 1LO phonon, 1LO phonon and 1TA phonon, and 1LO phonon and 1TO phonon with emission peaks at  $E_g - E_x - E_{BX} - 1\text{LO}(T) = 5.734$  eV,  $E_g - E_x - E_{BX} - 1\text{LO}(T) - 1\text{TA}(T) = 5.677$  eV, and  $E_g - E_x - E_{BX} - 1\text{LO}(T) - 1\text{TO}(T) = 5.581$  eV, respectively.

Second, zero-phonon lines (ZPLs) of the free-exciton (FX) and bound-exciton (BX) transitions become allowed in h-BN epilayers and appear as weak peaks at  $E_g - E_x = 5.958$  eV and  $E_g - E_x - E_{BX} = 5.917$  eV, respectively. At first sight, this seems contradictory to the requirement of momentum conservation since the h-BN is an indirect energy bandgap semiconductor. However, it is known that the momentum conservation requirement can be relaxed due to symmetry-breaking in the presence of impurities/defects and strain. A previous theoretical study has provided insights that when taking symmetry-breaking effects such as dislocations or defects into consideration, the lowest-lying exciton, which is “dark” for the perfect h-BN crystal, can acquire some oscillator strength.<sup>26</sup> The h-BN epilayers studied here contain carbon impurities and crystal defects and are also under strain, as revealed by XRD, SIMS, and Raman results shown in Fig. 1. Indeed, the zero-phonon line of the free exciton transition appearing at 5.96 eV has been observed previously in h-BN epilayers grown by CVD using carbon-free precursors.<sup>23</sup> On the other hand, a direct exciton transition at 5.955 eV involving zero-phonons in h-BN bulk materials was also observable via a two-photon excitation spectroscopy measurement technique.<sup>20</sup>

For the “band-to-band” group of emission lines, we attribute the emission line at 6.150 eV to the direct observation of the zero-phonon line of the band-to-band transition involving the CBM at M-point and VBM at K-point in the first BZ, which has never been reported previously. Again, this transition is expected to be forbidden or “dark.” The reason for this assignment is that the phonons involved in the replica lines at 6.069, 6.039, and 6.008 eV are all related to K- and M-points in the first BZ. Figures 3(a) and 3(b) are conceptual illustrations of possible scenarios facilitating the observation of the band-to-band transitions. While the exciton wavefunction extends beyond one unit cell in the c-plane, giving rise to a wavefunction spread over the entire first BZ in the reciprocal space as illustrated in Fig. 3(c), the wavefunctions of electrons and holes are all very localized in the k-space at M- and K-points, respectively, as illustrated in Fig. 3(d). Consequently, the band-to-band transitions assisted by phonons either at the M-point via an electron–phonon interaction [Fig. 3(a)] or at the K-point via a hole–phonon interaction

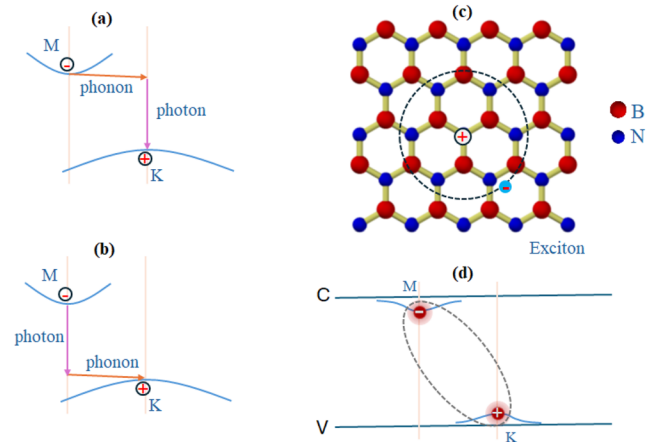


**FIG. 3.** (a) and (b) Illustrations of possible scenarios facilitating the band-to-band transitions, which can occur via an electron–phonon interaction at M-point (a) or via a hole–phonon interaction at K-point. (b) Electrons and holes are localized at the conduction and valence band extremes at the M- and K-points in the BZ, respectively. The band-to-band transition can only be assisted by phonons at M-point via an electron–phonon interaction or at K-point via a hole–phonon interaction. (c) Illustration of exciton in the c-plane of h-BN. The Bohr radius of exciton in h-BN is larger than the size of one unit cell, and its wavefunction extends in the k-space and covers the entire first BZ in the k-space. (d) Illustration of electron and hole wavefunctions at the conduction and valence band extremes at M- and K-points in the BZ, respectively, in h-BN. Even with the requirement of momentum conservation relaxed due to symmetry-breaking in the presence of impurities, defects, and strain, phonon assisted optical transitions are expected to be overwhelmingly dominant over the zero-phonon line.

[Fig. 3(b)] are still overwhelmingly dominant over the zero-phonon line.

The direct observation of the zero-phonon line of the band-to-band emission line enables the determination of the exciton binding energy,  $E_x$ , in h-BN epilayers, which is  $E_x = (6.150 - 5.958)$  eV = 0.192 eV. Attempts have been made earlier to determine the free exciton binding energy in h-BN experimentally using materials grown by different methods and measurement techniques,<sup>16–24,33–35</sup> yielding a large variation in the value of  $E_x$ . Using two-photon spectroscopy measurements, the exciton binding energy in h-BN bulk materials was determined to be about 130 meV.<sup>20</sup> The value of  $E_x = 0.192$  eV obtained for h-BN epilayers here seems very reasonable considering the epilayers studied here are under strain. Moreover, the direct observation of the impurity bound exciton transition at 5.917 eV also provides a value of the binding energy of impurity bound exciton,  $E_{BX} = 5.958 - 5.917$  eV = 0.041 eV. The nature of impurities involved in the impurity bound exciton transition is most likely carbon. It is worth emphasizing that there is a continuing need to investigate the basic parameters of h-BN, including the energy bandgap ( $E_g$ ), exciton binding energy ( $E_x$ ), and binding energy of impurity bound excitons ( $E_{BX}$ ), as different types of materials contain varying concentrations of defects and degrees of strain, all of which can influence the measured values.

Table II summarizes the basic parameters obtained from epilayers grown by MOCVD studied here as well as by the carbon-free

**TABLE II.** Comparison of excitonic parameters of h-BN epilayers and bulk materials obtained by PL emission spectroscopy.

Materials	High-purity bulk <sup>16–20,34</sup>	Epilayer <sup>23</sup>	Epilayer (this work)
Growth method	HPHT or metal flux solution	Carbon-free CVD	MOCVD
B source	BN powder	BCl <sub>3</sub>	TEB
Contain residual C element	No	No	Yes
Strain	Minimal	Yes	Yes
Main PL lines (eV)	5.77, 5.89 <sup>20</sup>	5.76, 5.79	5.734
Origin of the main PL lines (FX = free exciton; BX = bound exciton)	FX + LO(T)/TO(T) <sup>20</sup>	FX + LO(T)/TO(T)	BX + LO(T)
FX peak position (eV)	5.955 <sup>20</sup>	5.96	5.958
Momentum conservation relaxed	Yes	Yes	Yes
$E_g$ (eV) @ 10 K, directly measured	N/A	N/A	6.150
FX binding energy, $E_x$ (meV) directly measured	130 <sup>20</sup>	N/A	192
Impurity BX binding energy, $E_{BX}$ (meV), directly measured	N/A	N/A	41

CVD method<sup>23</sup> and high purity bulk materials.<sup>20</sup> One major difference between bulk materials and epilayers is that the crystalline quality is generally higher for h-BN bulk materials. Another important characteristic of the h-BN epilayers studied here is that they contain residual carbon impurities, whereas h-BN bulk materials and epilayers grown by carbon-free CVD are expected to contain no residual carbon impurities. Furthermore, the degrees of strain in these materials are all different, with h-BN epilayers grown on sapphire expected to possess larger stresses than the bulk materials. The presence of strain will also slightly affect the measured values of the  $E_g$  and  $E_x$ . The observation of a bound exciton transition being the dominant emission instead of a free exciton transition in the h-BN epilayers studied here is due to the presence of carbon impurities incorporated from the TEB source during growth. Being an indirect bandgap semiconductor with a conduction (valence) band extremum at the M- (K-) point in the BZ, exciton and band-to-band transitions in perfect h-BN crystals occur via phonon scattering to satisfy the momentum conservation. The direct observations of zero-phonon lines of the exciton and band-to-band transition in the epilayers studied here suggest that the conservation of momentum is relaxed due to symmetry-breaking in the presence of impurities/defects and strain. This interpretation is corroborated by the observation of the zero-phonon line of the free exciton transition at 5.96 eV in the h-BN epilayer grown by a carbon-free CVD growth method,<sup>23</sup> as both types of epilayers possess relatively lower crystalline quality and higher strain than the bulk materials. In more extreme cases of other 2D materials, such as germanium, the presence of strain can even lead to direct to indirect bandgap transitions.<sup>36,37</sup>

In summary, we have measured and analyzed a low temperature PL emission spectrum obtained in the band-edge region for h-BN epilayers grown by MOCVD using a TEB source. The band-to-band, free exciton, and impurity bound exciton transitions involving zero-phonons have been directly observed. From the observed peak positions of these fundamental transition lines, important parameters including the energy bandgap ( $E_g$ ), exciton binding energy ( $E_x$ ), and binding energy of impurity bound excitons ( $E_{BX}$ ) have been directly determined. Optical properties and parameters of h-BN grown by different methods are also summarized and compared. These results provide a more coherent understanding of

fundamental optical transitions in h-BN, which are of paramount importance for further advancing h-BN material and device technologies.

The information, data, or work presented herein was funded in part by the Advanced Research Projects Agency-Energy (ARPA-E), U.S. Department of Energy, under Award No. DE-AR0001552, monitored by Dr. Olga Spahn and Dr. Eric Carlson. The views and opinions of authors expressed herein do not necessarily state or reflect those of the United States Government or any agency thereof. Jiang and Lin are grateful to the AT&T Foundation for the support of Ed Whitacre and Linda Whitacre endowed chairs.

## AUTHOR DECLARATIONS

### Conflict of Interest

The authors have no conflicts to disclose.

### Author Contributions

**J. Li:** Conceptualization (equal); Data curation (equal); Formal analysis (equal); Funding acquisition (equal); Investigation (equal); Methodology (equal); Project administration (equal); Resources (equal); Software (equal); Supervision (equal); Validation (equal); Visualization (equal). **J. Y. Lin:** Conceptualization (equal); Formal analysis (equal); Funding acquisition (equal); Investigation (equal); Methodology (equal); Project administration (equal); Resources (equal); Supervision (equal); Validation (equal); Visualization (equal); Writing – review & editing (equal). **H. X. Jiang:** Conceptualization (equal); Formal analysis (equal); Funding acquisition (equal); Investigation (equal); Methodology (equal); Project administration (equal); Resources (equal); Supervision (equal); Validation (equal); Visualization (equal); Writing – original draft (equal); Writing – review & editing (equal).

### DATA AVAILABILITY

The data that support the findings of this study are available within the article.

## REFERENCES

- <sup>1</sup>N. Alem, R. Erni, C. Kisielowski, M. D. Rossell, W. Gannett, and A. Zettl, *Phys. Rev. B* **80**, 155425 (2009).
- <sup>2</sup>L. Song, L. Ci, H. Lu, P. B. Sorokin, C. Jin, J. Ni, A. G. Kvashnin, D. G. Kvashnin, J. Lou, B. I. Yakobson, and P. M. Ajayan, *Nano Lett.* **10**, 3209 (2010).
- <sup>3</sup>R. V. Gorbachev, I. Riaz, R. R. Nair, R. Jalil, L. Britnell, B. D. Belle, E. W. Hill, K. S. Novoselov, K. Watanabe, T. Taniguchi, A. K. Geim, and P. Blake, *Small* **7**, 465 (2011).
- <sup>4</sup>T. T. Tran, C. Elbadawi, D. Totonjian, C. J. Lobo, G. Grosso, H. Moon, D. R. Englund, M. J. Ford, I. Aharonovich, and M. Toth, *ACS Nano* **10**, 7331 (2016).
- <sup>5</sup>N. R. Jungwirth, B. Calderon, Y. Ji, M. G. Spencer, M. E. Flatté, and G. D. Fuchs, *Nano Lett.* **16**, 6052 (2016).
- <sup>6</sup>Z. Shotan, H. Jayakumar, C. R. Considine, M. Mackoito, H. Fedder, J. Wrachtrup, A. Alkauskas, M. W. Doherty, V. M. Menon, and C. A. Meriles, *ACS Photonics* **3**, 2490 (2016).
- <sup>7</sup>K. Watanabe, T. Taniguchi, and H. Kanda, *Nat. Mater.* **3**, 404 (2004).
- <sup>8</sup>Y. Kubota, K. Watanabe, O. Tsuda, and T. Taniguchi, *Science* **317**, 932 (2007).
- <sup>9</sup>S. Majety, J. Li, X. K. Cao, R. Dahal, B. N. Pantha, J. Y. Lin, and H. X. Jiang, *Appl. Phys. Lett.* **100**, 061121 (2012).
- <sup>10</sup>D. A. Laleyan, W. Lee, Y. Zhao, Y. Wu, P. Wang, J. Song, E. Kioupakis, and Z. Mi, *APL Mater.* **11**, 051103 (2023).
- <sup>11</sup>A. Maity, S. J. Grenadier, J. Li, J. Y. Lin, and H. X. Jiang, *Appl. Phys. Lett.* **116**, 142102 (2020).
- <sup>12</sup>A. Tingsuwatit, A. Maity, S. J. Grenadier, J. Li, J. Y. Lin, and H. X. Jiang, *Appl. Phys. Lett.* **120**, 232103 (2022).
- <sup>13</sup>Z. Alemoush, A. Tingsuwatit, A. Maity, J. Li, J. Y. Lin, and H. X. Jiang, *J. Appl. Phys.* **135**, 175704 (2024).
- <sup>14</sup>A. Mballo, A. Ahaitouf, S. Sundaram, A. Srivastava, V. Ottapilakkal, R. Gujrati, P. Vuong, S. Karrakchou, M. Kumar, X. Li, Y. Halfaya, S. Gautier, P. L. Voss, J. P. Salvestrini, and A. Ougazzaden, *ACS Omega* **7**, 804 (2022).
- <sup>15</sup>O. Slobodyan, J. Flicker, J. Dickerson, J. Shoemaker, A. Binder, T. Smith, S. Goodnick, R. Kaplar, and M. Hollis, *J. Mater. Res.* **37**, 849 (2022).
- <sup>16</sup>K. Watanabe and T. Taniguchi, *Phys. Rev. B* **79**, 193104 (2009).
- <sup>17</sup>K. Watanabe, T. Taniguchi, T. Kuroda, O. Tsuda, and H. Kanda, *Diamond Relat. Mater.* **17**, 830 (2008).
- <sup>18</sup>X. K. Cao, B. Clubine, J. H. Edgar, J. Y. Lin, and H. X. Jiang, *Appl. Phys. Lett.* **103**, 191106 (2013).
- <sup>19</sup>J. Li, X. K. Cao, T. B. Hoffman, J. H. Edgar, J. Y. Lin, and H. X. Jiang, *Appl. Phys. Lett.* **108**, 122101 (2016).
- <sup>20</sup>G. Cassaboïs, P. Valvin, and B. Gil, *Nat. Photon* **10**, 262 (2016).
- <sup>21</sup>G. Cassaboïs, P. Valvin, and B. Gil, *Phys. Rev. B* **93**, 035207 (2016).
- <sup>22</sup>T. Q. P. Vuong, G. Cassaboïs, P. Valvin, V. Jacques, R. Cusco, L. Artus, and B. Gil, *Phys. Rev. B* **95**, 045207 (2017).
- <sup>23</sup>S. F. Chichibu, K. Shima, K. Kikuchi, N. Umehara, K. Takiguchi, Y. Ishitani, and K. Hara, *Appl. Phys. Lett.* **120**, 231904 (2022).
- <sup>24</sup>X. Z. Du, J. Li, J. Y. Lin, and H. X. Jiang, *Appl. Phys. Lett.* **108**, 052106 (2016).
- <sup>25</sup>B. Arnaud, S. Lebègue, P. Rabiller, and M. Alouani, *Phys. Rev. Lett.* **96**, 026402 (2006).
- <sup>26</sup>L. Wirtz, A. Marini, M. Gruning, C. Attaccalite, G. Kresse, and A. Rubio, *Phys. Rev. Lett.* **100**, 189701 (2008).
- <sup>27</sup>L. Artús, M. Feneberg, C. Attaccalite, J. H. Edgar, J. Li, R. Goldhahn, and R. Cuscó, *Adv. Photonics Res.* **2**, 2000101 (2021).
- <sup>28</sup>R. S. Pease, *Acta Cryst.* **5**, 356 (1952).
- <sup>29</sup>B. Heying, X. H. Wu, S. Keller, Y. Li, D. Kapolnek, B. P. Keller, S. P. DenBaars, and J. S. Speck, *Appl. Phys. Lett.* **68**, 643 (1996).
- <sup>30</sup>Y. Li, V. Garnier, P. Steyer, C. Journet, and B. Toury, *ACS Appl. Nano Mater.* **3**, 1508 (2020).
- <sup>31</sup>Q. Cai, D. Scullion, A. Falin, K. Watanabe, T. Taniguchi, Y. Chen, E. J. G. Santos, and L. H. Li, *Nanoscale* **9**, 3059 (2017).
- <sup>32</sup>J. Serrano, A. Bosak, R. Arenal, M. Krisch, K. Watanabe, T. Taniguchi, H. Kanda, A. Rubio, and L. Wirtz, *Phys. Rev. Lett.* **98**, 095503 (2007).
- <sup>33</sup>T. C. Doan, J. Li, J. Y. Lin, and H. X. Jiang, *Appl. Phys. Lett.* **109**, 122101 (2016).
- <sup>34</sup>L. Schué, L. Sponza, A. Plaud, H. Bensalah, K. Watanabe, T. Taniguchi, F. Ducastelle, A. Loiseau, and J. Barjon, *Phys. Rev. Lett.* **122**, 067401 (2019).
- <sup>35</sup>S. Roux, C. Arnold, F. Paleari *et al.*, *Phys. Rev. B* **104**, L161203 (2021).
- <sup>36</sup>Y. Hoshina, K. Iwasaki, A. Yamada, and M. Konagai, *Jpn. J. Appl. Phys.* **48**, 04C125 (2009).
- <sup>37</sup>S. B. Desai, G. Seol, J. S. Kang, H. Fang, C. Battaglia, R. Kapadia, J. W. Ager, J. Guo, and A. Javey, *Nano Lett.* **14**, 4592 (2014).